

## Enhancing surface properties and corrosion resistance of API 5L X52 steel through orthogonal ball burnishing

Selma Belabend, Hamid Hamadache, Quang Phamdonhat

Online Publication Date: 10 October 2023

URL: <http://www.jresm.org/archive/resm2023.833ma0725.html>

DOI: <http://dx.doi.org/10.17515/resm2023.833ma0725>

Journal Abbreviation: *Res. Eng. Struct. Mater.*

### To cite this article

Belabend S, Hamadache H, Phamdonhat Q. Enhancing surface properties and corrosion resistance of API 5L X52 steel through orthogonal ball burnishing. *Res. Eng. Struct. Mater.*, 2024; 10(1): 233-251.

### Disclaimer

All the opinions and statements expressed in the papers are on the responsibility of author(s) and are not to be regarded as those of the journal of Research on Engineering Structures and Materials (RESM) organization or related parties. The publishers make no warranty, explicit or implied, or make any representation with respect to the contents of any article will be complete or accurate or up to date. The accuracy of any instructions, equations, or other information should be independently verified. The publisher and related parties shall not be liable for any loss, actions, claims, proceedings, demand or costs or damages whatsoever or howsoever caused arising directly or indirectly in connection with use of the information given in the journal or related means.



Published articles are freely available to users under the terms of Creative Commons Attribution - NonCommercial 4.0 International Public License, as currently displayed at [here](https://creativecommons.org/licenses/by-nc/4.0/) (the "CC BY - NC").

## Enhancing surface properties and corrosion resistance of API 5L X52 steel through orthogonal ball burnishing

Selma Belabend<sup>1, a</sup>, Hamid Hamadache<sup>1, b</sup>, Quang Phamdonhat<sup>2, c</sup>

<sup>1</sup>Research Laboratory of Advanced Technology in Mechanical Production (LRATPM), Mechanical Eng. Dept., Faculty of Technology, Badji Mokhtar-Annaba University, Algeria

<sup>2</sup>Sarl Ava Cristal, 12 Latham Beau Séjour, 23000 Annaba, Algeria

### Article Info

#### Article history:

Received 25 July 2023

Accepted 01 Oct 2023

#### Keywords:

Burnishing;  
Corrosion;  
Microhardness;  
Surface roughness;  
Steel X52;  
Taguchi method

### Abstract

Surface engineering involves using various technologies to modify the surface and near-surface areas of a material to enable it to perform different functions from the bulk of the material. Two primary methods of surface engineering are surface coatings and surface modification. Orthogonal ball burnishing is a process that improves certain surface integrity properties of materials through superficial plastic deformation. This study focuses on the effect of this treatment and the influence of its parameters on the physico-geometric surface characteristics of API 5L X52 steel. Burnishing tests were conducted with four main parameters: burnishing force (Py), feed rate (f), spindle speed (N), and number of passes (i). The analysis revealed an appropriate combination of burnishing parameters that led to a 98% reduction in surface roughness and a 42% increase in surface microhardness. A multi-objective optimization of roughness and microhardness after burnishing yielded optimal parameters. Furthermore, a multifactorial experimental design demonstrated that corrosion resistance increased by 318%.

© 2024 MIM Research Group. All rights reserved.

## 1. Introduction

Deterioration of structural elements is caused by mechanical interactions, contact with other elements, exposure to aggressive environments and exposure to dynamic loads. This necessitates the modification of surface layers to enhance properties and meet high technical standards, with a particular emphasis on strength and corrosion resistance [1,2]. Despite considerable efforts to ensure their safety and reliability, pipeline failures still occur. The primary mode of failure is leakage or rupture caused by cracks and defects in the pipes during their production process or corrosion during their service life. Such defects can compromise the integrity of the pipeline and pose serious safety risks [3]. Failure on the outer surface of oil and gas pipelines is a significant concern [4,5]. Several studies have investigated the causes and consequences of pipeline failures. Song et al [6] found that the leakage and ignition of a carbon steel pipeline were mainly due to local electrochemical corrosion. Ranjbar and Alavi Zaree [7] identified pitting corrosion as the primary failure mechanism in a micro alloyed steel pipeline, caused by the accumulation of corrosion products and water separation. Assessment of oil and gas pipeline failure in Vietnam has been studied by Dao U et al [8]. They propose a model that integrates Fault Tree Analysis (FTA) and fuzzy theory to analyze the causes of pipeline failure and evaluate the level of uncertainty using Monte Carlo simulation. The study identifies twenty-one risk factors that lead to pipeline failure, with rupture being the highest risk, followed by puncture. Corrosion has lower chances of pipeline failure but carries catastrophic

\*Corresponding author: [selma.belabend@univ-annaba.dz](mailto:selma.belabend@univ-annaba.dz)

<sup>a</sup> [orcid.org/0009-0006-0033-6040](https://orcid.org/0009-0006-0033-6040), <sup>b</sup> [orcid.org/0000-0002-3373-5738](https://orcid.org/0000-0002-3373-5738), <sup>c</sup> [orcid.org/0009-0003-3820-7218](https://orcid.org/0009-0003-3820-7218)

DOI: <https://dx.doi.org/10.17515/resm2023.833ma0725>

Res. Eng. Struct. Mat. Vol. 10 Iss. 1 (2024) 233-251

consequences. To prevent such occurrences, it is essential to ensure high-quality surface finishes for these products. In this regard, surface integrity is widely used as a quality criterion or for comparison purposes among different materials or different states of the same material. Such properties strongly depend on the quality of the surface finish. However, it has been found that regardless of the manufacturing technology (e.g., machining, heat treatment), on the one hand, the surface layers can be overloaded due to residual tensile stresses that add to the service stresses, and on the other hand, all mechanical surfaces consist of irregular pits and valleys with varying heights and spacing [9], which can act as sites for corrosion or stress concentration. Therefore, these surfaces undergo surface finishing processes that can improve their physical-geometric properties in terms of microhardness and roughness [5-6].

One increasingly used solution in surface engineering is to integrate surface treatment operations into the production process of structural elements. Burnishing is one such surface treatment operation that is gradually being used as a finishing process to quickly generate high-quality surfaces, offering additional benefits to surface integrity [12]. The process can be easily executed without chip removal on both universal and CNC machine tools [13]. In this regard, various tool designs have emerged, ranging from simple devices to tools assisted by vibrations or ultrasonics [9-10], enabling process automation and increased production rates [16]. In all cases, the generated surface results from a controlled and carefully applied pressure using a ball or roller, without any change in volume, structure, or chemical composition of the material to impart specific physical, mechanical, and tribological properties [17]. The process provides good corrosion resistance and improved fatigue life [18]. A literature review has shown that numerous experimental studies have been conducted to identify the effects of burnishing on surface quality and surface microhardness. Surface roughness, after ball burnishing treatment, can be improved by 40% to 90%, while hardness can be increased by 5% to 160% [16,19]. A multi-objective optimization of process parameters for low plasticity burnishing on aluminum alloy AA6061T6 was performed by Thorat et al [20]. The burnishing process parameters considered were pressure, speed, ball diameter, ball material, and number of passes. Kovács et al. [21] applied Magnetic Assisted Ball Burnishing (MABB) to enhance the hardness and decrease the roughness of machined parts made of C45 steel. Through Taguchi method optimization, they discovered that the corrosion rate is greatly influenced by the burnishing speed and strategy. Al-Qawabeha et al. [22] conducted research on the influence of burnishing on A53 steel. Their study revealed that the corrosion rate decreased with an increase in applied force up to 80 N. However, exceeding this threshold force resulted in an escalation of the corrosion rate. The ball burnishing process has been extensively studied, with parameters such as speed, feed rate, burnishing force, ball diameter, and lubricant type under investigation. These parameters have been found to have significant effects on various aspects of the burnishing process, including surface roughness, residual stresses, microhardness, plastic strain, phase transformation, elastic recovery effect, ball indentation mark, and thermal behavior of the workpiece. Additionally, process parameters also influence the surface integrity of the workpiece, affecting properties such as corrosion resistance, wear resistance, fatigue life, and dimensional tolerances [23–25]. Four critical factors—burnishing force ( $P_y$ ), feed rate ( $f$ ), spindle speed ( $N$ ), and the number of passes ( $i$ )—were investigated to assess their influence on the surface roughness and microhardness of the outer surface of the pipeline material. The authors of this study based their selection burnishing parameters on well-established guidance from the existing literature [25–27].

By employing a robust combination of Taguchi L16 to analyse the effect of ball burnishing parameters on roughness and microhardness, and a comprehensive full-factorial design study was executed to meticulously evaluate the effects of burnishing parameters on corrosion resistance. Additionally, to gain deeper insights into corrosion resistance, Response Surface Methodology (RSM) was adeptly employed alongside regression

analysis. These analytical tools collectively facilitated the development of a precise linear model capable of predicting the behaviour of essential parameters, including surface roughness (Ra), microhardness ( $\mu\text{Hv}$ ), and, significantly, corrosion resistance (Rp). The incorporation of ANOVA provided essential statistical insights into the impact of these parameters on the overall performance of the material.

Furthermore, to optimize the material properties, a Desirability Function Approach (DFA) was employed. This optimization technique aimed to maximize microhardness while simultaneously minimizing surface roughness. The integration of DFA further enhanced the study's ability to fine-tune the burnishing process for superior material performance.

## 2. Experimental Details

### 2.1. Material

The material used in this study is API 5L X52 steel, which is commonly used in the oil and gas industries. It is a high yield strength low alloy steel that meets the specification requirements of the API 5L standard [28]. To perform spectral examination of the material, spectrometry (OLYMPUS optical microscope) was utilized, which resulted in the chemical composition as follows (Table 1).

Table 1. Chemical composition of API 5L X52 steel [29]

Compound	C	Mn	Si	P	S	Cu	Ni	Cr
%	0.16	1.33	0.22	0.010	0.002	0.033	0.013	0.047

The mechanical properties of the steel were assessed using tensile testing conducted at room temperature. Prismatic specimens were meticulously prepared in accordance with the ASTM A370 standard [28], ensuring precision and consistency in the testing process. A total of six tests were carried out on the steel specimens, and the subsequent analysis yielded the following average mechanical properties: the yield strength (Re) was determined to be 439.24 MPa, while the ultimate tensile strength (UTS) was measured at 575.5 MPa. Additionally, the elongation at rupture (A%) was calculated to be 35.6. The steel was subjected to six tests, and the resulting average properties were evaluated. Specifically, the initial surface condition was characterized by a roughness of  $R_a = 2.82 \mu\text{m}$  and a microhardness of  $\mu\text{Hv} = 188$  [29].

### 2.2. Burnishing

In order to guarantee the inclusiveness of industrial structures, samples were collected longitudinally from a pipeline. The preliminary surface preparation was conducted by employing a vertical milling machine, more precisely an HMT India Type, which was outfitted with a carbide metal end mill. To facilitate the implementation of the burnishing treatment, as per the experimental design methodology, the sample was partitioned into zones with the aid of grooves that had a width of 50 mm and a depth of 2 mm, as depicted in Figure 1[29].

The mechanical treatment of the specimens was executed through the utilization of a ball burnishing instrument on a vertical milling apparatus. To achieve this, a purpose-specific burnishing tool was designed, as illustrated in Figure 2. The system comprises a sturdy steel ball that is affixed to a shaft which glides within a hub of the tool holder. The applied force is measured with a load spring calibrated to a specific value. The burnishing system is then mounted on the spindle to be subjected to vertical displacement. The burnishing procedure begins by exerting force with the ball onto the surface of a part, thereby causing a corresponding plastic deformation on a point of the external layer. The ball is then

scanned across the entire surface in order to complete the burnishing operation[30]. In this investigation of ball burnishing of API 5L X52 steel, the mechanical surface treatment was performed on the exterior surface of the pipeline.

For this study, a bespoke static device with interchangeable heads was meticulously designed. This device is capable of treating both cylindrical and prismatic surfaces. A patent application (No.: DZ/P/2023/000830) for this apparatus was filed on 18/06/2023.

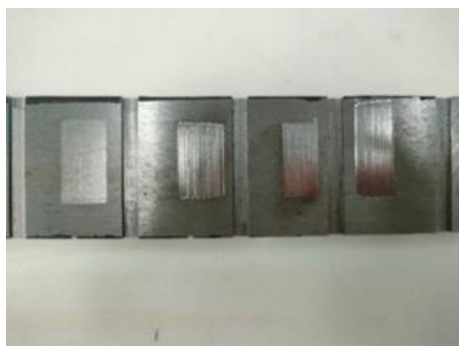


Fig. 1. Sample preparation [29]



Fig. 2. Setup photo of the burnishing operation[29]

Roughness was measured at three distinct locations on the machined surface using a Cyber Technology CT100 laser source profilometer. The measurements were repeated three times, and the average values were recorded. Microhardness of the samples was measured using a Matsuzawa MXT70 microhardness tester with a 200-gf load applied for 10 seconds. Similarly, measurements were taken at three different zones, and the average value was considered as the test result. Table 2 summarizes the test results along with the corresponding signal-to-noise (S/N) ratios.

Table 2. Taguchi Matrix of Measured Values for Ra and  $\mu\text{Hv}$

N°	Py	f	N	i	Ra	$\mu\text{Hv}$
1	265	300	560	1	0.18	236
2	265	400	730	3	0.17	254
3	265	500	900	5	0.15	250
4	265	600	1070	7	0.13	230
5	347.5	300	730	5	0.09	239
6	347.5	400	560	7	0.07	245
7	347.5	500	1070	1	0.12	239
8	347.5	600	900	3	0.05	211
9	430	300	900	7	0.26	246
10	430	400	1070	5	0.14	229
11	430	500	560	3	0.22	267
12	430	600	730	1	0.14	211
13	512.5	300	1070	3	0.12	223
14	512.5	400	900	1	0.14	205
15	512.5	500	730	7	0.15	218
16	512.5	600	560	5	0.11	214

### 2.3. Corrosion Test

There are several techniques to determine corrosion rates, including electrochemical impedance spectroscopy (EIS), electrochemical linear polarization resistance (LPR), and the weight loss technique. For the electrochemical analysis, a Gamry 600+ cell controlled by a microcomputer was utilized to investigate the electrochemical properties. Corrosion tests were conducted on samples coated with acrylic resin to improve adhesion. The samples were cleaned in an ultrasonic tank and dried with acetone prior to coating. The examination specimens were arranged in a three-electrode configuration, consisting of a reference electrode, a counter electrode, and a working electrode. These specimens were then immersed in a concentrated 3.5% NaCl aqueous solution of distilled water (Fig 3). The electrochemical linear polarization resistance (LPR) technique was employed as part of this study to assess the corrosion behavior of the specimens[31,32]. The electrochemical linear polarization resistance (LPR) technique can be used for corrosion monitoring and control in various applications. It is a method that measures the resistance of a material to corrosion by applying a small potential to the material and measuring the resulting current. LPR can be used to validate the corrosion rate obtained from other methods, such as the impressed current method, and can provide a more accurate quantification of the actual mass loss rate of steel in natural environments[33–35].

Electrochemical corrosion tests were performed at room temperature. The corrosion potential ( $E_{corr}$ ) was set within the range of -0.8 to -0.3 mV, and the scanning rate was set at 1 mA/s. However, the immersion time of the samples in the saline solution was limited to 30 minutes to record the OCP (Open Circuit Potential) curves, while it was extended to 20 minutes for the Tafel curves. Corrosion resistance was characterized by the corrosion potential ( $E_{corr}$ ), corrosion current ( $I_{corr}$ ), and the potential ( $\beta$ ) between the cathode and anode. Such measurements were directly obtained using the GAMRY software, which controlled the electrochemical cell.

### 2.4. Methodology

Taguchi techniques are a strategy that uses simulation to optimize parameters and reduce



Fig. 3. Corrosion test Gamry 600+ cell [29]

solution space in various fields. To optimize the number of simulations required, they involve a sequence of experiments to narrow down the combinations of factors and levels. The Taguchi orthogonal array design matrix is used by the technique to determine the most significant factors that influence the performance parameter of interest. The analysis of variance (ANOVA) is then used to identify the contribution of each factor. Taguchi

method consists of three steps: design of experiments (DOE), signal-to-noise (S/N) ratio analysis, and optimization. In the DOE step, a set of experiments is designed to investigate the effects of several factors on the performance of the process. The experiments are designed based on orthogonal arrays, which are a set of systematically arranged test cases that allow for the efficient and effective identification of the most significant factors. Orthogonal arrays reduce the number of experiments required while ensuring that all factors are evaluated at different levels [36,37]

Table 3 shows the configuration of the burnishing parameters and their levels for roughness and microhardness tests. These parameters were combined with each other in accordance with Taguchi's orthogonal plane L16 (Table 2).

Table 3. Factors and their levels for the experiments

Burnishing Parameters	Level			
	1	2	3	4
Py	265	347.5	430	512.5
f	300	400	500	600
N	560	730	900	1070
i	1	3	5	7

The design of the experimental design was optimized by the signal-to-noise ratio (S/N). This report is widely used as an objective function to solve engineering design problems [3]. The signals adopted for this study are such as "smaller is better" for roughness (Eq. 1) and "larger is better" for microhardness (Eq. 2).

$$\eta_s = -10 \log \left( \frac{1}{n} \sum_i^n y_i^2 \right) \tag{1}$$

$$\eta_l = -10 \log \left( \frac{1}{n} \sum_i^n \frac{1}{y_i^2} \right) \tag{2}$$

where, yi: the ith result of the experiment. n: the repeated number of the ith experiment

The experimental corrosion tests were conducted using a multifactorial design of full experiments. Two burnishing parameters, Py and f, were selected for this purpose, with two levels (low and high) assigned to each parameter. The burnishing was conducted with one pass and at 900 rpm. To facilitate analysis, the factors were translated into reduced focused variables, denoted as X1 and X2. The coding scheme employed in this study utilized (-1) to represent the low levels and (+1) to represent the high levels. A series of 4 trials were conducted, during which the factor levels were systematically combined based on the prescribed design and matrix of experiments. (Table 4).

Table 4. Factors and their levels for the experiments for the corrosion test

N	Natural Value		Coded Value	
	Py	f	X1	X2
1	265	400	-1	-1
2	265	500	-1	+1
3	430	400	+1	-1
4	430	500	+1	+1

### 3. Results and Discussion

#### 3.1. Effect of Burnishing on Surface Roughness and Microhardness

The effect of burnishing on Ra and  $\mu\text{Hv}$  was evaluated through the analysis of the signal-to-noise (S/N) ratio (Table 2). Under certain conditions, burnishing resulted in a surface topography characterized by Ra values ranging from 0.05 to 0.26  $\mu\text{m}$  Figure 4 and 5.

The effect of each variable on the output response (Ra and  $\mu\text{Hv}$ ) is estimated using the S/N ratio for each experiment (Table 2). However, analyzing average S/N ratio by factor levels (Table 5) reveals that the optimal burnishing conditions for roughness are provided by level 2 of the burnishing force, level 4 of the feed rate and spindle speed, and level 3 of the number of tool passes. The corresponding actual values for this combination are as follows:  $P_y = 347.5 \text{ N}$ ,  $f = 600 \text{ mm/min}$ ,  $N = 1070 \text{ rpm}$ , and  $i = 5$ . The most significant effects (according to the RANK) are those of  $P_y$  and  $f$ .

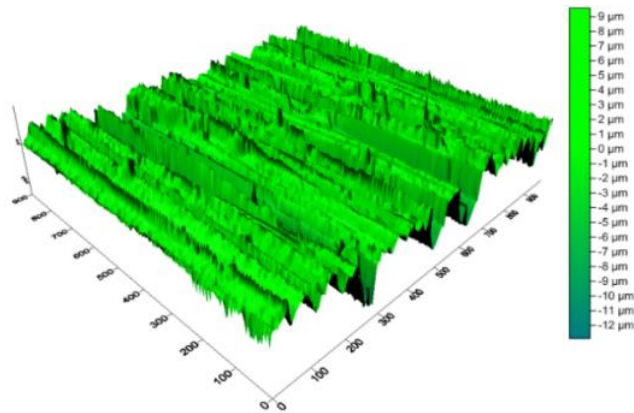


Fig. 4. Example of surface topography: before burnishing

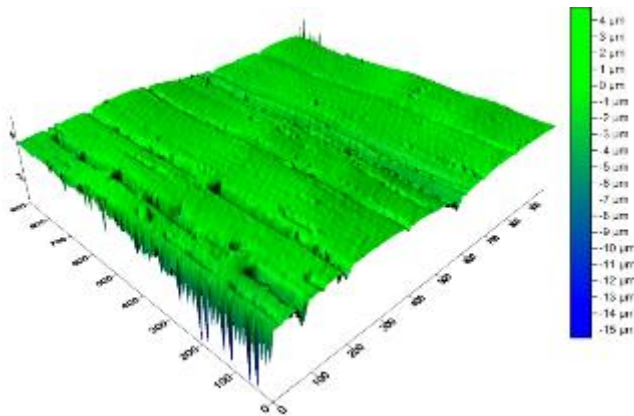


Fig. 5. Example of surface topography: after burnishing

Similarly, analyzing the S/N ratio for each level of parameters for surface microhardness reveals an optimal combination characterized by low levels of  $P_y$  and spindle speed (N), level 3 of the feed rate (f), and level 2 of the number of passes (i). The corresponding actual values for this combination are as follows:  $P_y = 265 \text{ N}$ ,  $f = 500 \text{ mm/min}$ ,  $N = 560 \text{ rpm}$ , and  $i = 3$ . According to the Rank in Table 5, it is also observed that  $P_y$  and  $f$  are the most

significant factors for microhardness. The effect of spindle speed is the least significant for both output responses.

Table 5. Average S/N Ratio by Level for Roughness (Ra) and Microhardness ( $\mu\text{Hv}$ )

Levels	S/N Ra				S/N $\mu\text{Hv}$			
	Py	f	N	i	Py	f	N	i
1	16.12	16.44	17.51	17.01	47.69	47.46	47.59	46.93
2	22.08	18.09	17.51	18.29	47.35	47.32	47.22	47.52
3	14.76	16.15	17.81	18.35	47.50	47.70	47.12	47.33
4	17.79	20.07	17.93	17.11	46.64	46.71	47.24	47.40
Delta	7.31	3.92	0.42	1.34	1.04	0.99	0.47	0.59
Rang	1	2	4	3	1	2	4	3

Figures 6 and 7 visually illustrate the primary effects of burnishing parameters on surface roughness and microhardness, respectively. In relation to both Ra and  $\mu\text{Hv}$ , the burnishing force (Py) seems to exert a substantial influence on the signal-to-noise ratio. Regarding Ra, the second level of Py is considered the most favorable, while for  $\mu\text{Hv}$ , the first level of Py is deemed the most desirable. Furthermore, the burnishing feed (f) also plays a significant role in both responses. When it comes to Ra, the fourth level of this parameter appears to be the most favorable, although the third level holds the greatest significance for  $\mu\text{Hv}$ . Consequently, N (Spindle Speed) has the least significant impact on both Ra and  $\mu\text{Hv}$ . Therefore N (Spindle Speed) has the least significant impact on both Ra and  $\mu\text{Hv}$ . The number of passes (i) shows some influence, but it varies in its effect on the two responses.

To optimize the burnishing process and achieve the desired balance between surface roughness (with the aim of minimizing it) and microhardness (with the objective of maximizing it), a composite optimization approach known as the Desirability Function Approach (DFA) is performed. DFA is a powerful tool because it enables the simultaneous optimization of multiple factors and responses. By assigning desirability values to different levels of each parameter and response, DFA provides a comprehensive perspective on process performance [38].

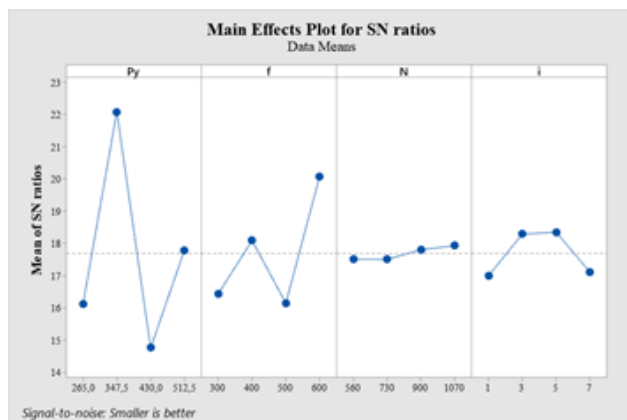


Fig. 6. Main effects of burnishing parameters Ra

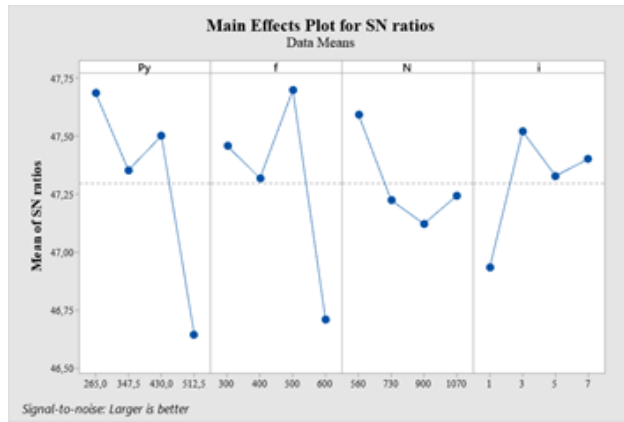


Fig. 7. Main effects of burnishing parameters  $\mu\text{Hv}$

### 3.2. ANOVA Analysis

To explore the impacts of burnishing process parameters in a quantitative manner, an Analysis of Variance (ANOVA) based on the Signal-to-Noise (S/N) ratio was utilized. An overview of the ANOVA outcomes for surface roughness is presented in Table 6, while Table 7 depicts the outcomes for microhardness. Following the ANOVA, a determination of the degree of influence of the parameters on the output was performed at a 95% confidence level via the calculation of the percentage contribution[37]. It can be observed from the ANOVA tables that burnishing force (60%) and feed rate (21%) play a significant role in minimizing surface roughness, whereas spindle speed (3%) and the number of passes (5%) do not exhibit notable effects on controlling surface roughness.

Table 6. Analysis of variance for surface roughness

Source	DF	Adj SS	Adj MS	F-Value	P-Value	Contribution %
Py	3	0.024850	0.008283	5.65	0.094	37%
f	3	0.008676	0.002892	1.97	0.296	32%
N	3	0.001247	0.000416	0.28	0.836	8%
i	3	0.001973	0.000658	0.45	0.737	12%
Error	3	0.004402	0.001467			11%
Total	15	0.041148				100%

This analysis shows that the burnishing force and feed rate are the most influential factors in reducing surface roughness, together accounting for (81%) of the variance. In contrast, spindle speed and the number of passes have minimal impact on surface roughness, contributing only (8%) in total.

Table 7. Analysis of variance for microhardness

Source	DF	Adj SS	Adj MS	F-Value	P-Value	Contribution %
Py	3	1754.4	584.8	3.54	0.163	60%
f	3	1519.9	506.6	3.07	0.191	21%
N	3	372.2	124.1	0.75	0.590	3%
i	3	562.4	187.5	1.14	0.459	5%
Error	3	495.0	165.0			11%
Total	15	4703.8				100%

ANOVA analysis for microhardness results indicates that the force applied (Py) and the feed rate (f) have a substantial impact on microhardness, contributing 37% and 32% to the variance, respectively. On the other hand, spindle speed (n) and the number of passes (i) show relatively lower contributions of 8% and 12%, respectively. The remaining unexplained variance is attributed to error, accounting for 11% of the total variance.

### 3.3 Regression Analysis

The regression analysis has yielded quadratic models to predict surface roughness (Eq. 3) and surface microhardness (Eq. 4) at any point within the study domain.

$$Ra = -13.83 + 0.03889Py + 0.006061 + 0.03369 N - 1.240 i - 0.000049 Py^2 - 0.000000 f^2 - 0.000017N^2 + 0.04531i^2 - 0.000002 Py \times f - 0.000005Py \times N + 0.000135Py \times i - 0.000020f \times N + 0.001000f \times i \tag{3}$$

$$\mu Hv = -1441 + 4.61 Py + 1.197 f + 3.152 N - 113.5 i - 0.00480 Py^2 - 0.000203 f^2 - 0.001144 N^2 + 3.50 i^2 - 0.000938 Pyf - 0.001461 Py \times N + 0.03467 Py \times i - 0.002064 f \times N + 0.0856 f \times i \tag{4}$$

The obtained models accurately characterize the respective output responses, as indicated by the high coefficient of determination (R<sup>2</sup>) values of 98.86% for surface roughness and 99.26% for microhardness. The quality of fit of the models to the experimental data is further validated by the adjusted determination coefficients (Raj<sup>2</sup>), which are approximately 91.43% and 94.44% for surface roughness and microhardness, respectively. The difference of less than 5% between these values indicates the absence of insignificant terms in the models [11].

### 3.4 Optimization and Validation of Results

To improve the corrosion resistance of the material post-treatment, it is imperative to find a compromise through the burnishing parameters that aim for both minimal roughness and maximum microhardness. Such an objective can be approached using the Desirability Function Approach (DFA). The considerable use of this approach is attributed to its simplicity, flexibility in weighting, and availability in the statistical software Minitab. When the responses are outside their acceptable limits (unacceptable value), the desirability is set to 0, while if the responses exactly coincide with the acceptable limits (target value), it is set to 1. Between these two values, the user has the discretion to assess, based on the responses calculated by the statistical model, the equivalent of a satisfaction percentage with respect to the set objectives. Therefore, the burnishing parameters need to be adjusted to approach the target value as closely as possible[38].

The significant utilization of this approach can be attributed to its simplicity, flexibility in weighting, and availability in statistical software. By assigning a value of +1 to the desired value (Ytarget) and a value of 0 to the unacceptable value (Yin), the desirability (di) can be expressed as follows: (Eq. 5).

$$d_i = \frac{y_i - y_{in}}{y_{target} - y_{in}} \tag{5}$$

Desirability allows for the evaluation of the level of satisfaction with regards to the established objectives, based on the responses obtained from the statistical model. Consequently, the global (composite) desirability can be expressed in the following form (Eq. 6):

$$D_i = [\sqrt{d_1 * d_2 * d_3 * d_4 * ... * d_n}]^{1/n} \tag{6}$$

If the value falls between 0 and 1, all the responses will be as close as possible to their target value, thus achieving the optimal compromise for the studied responses [38].

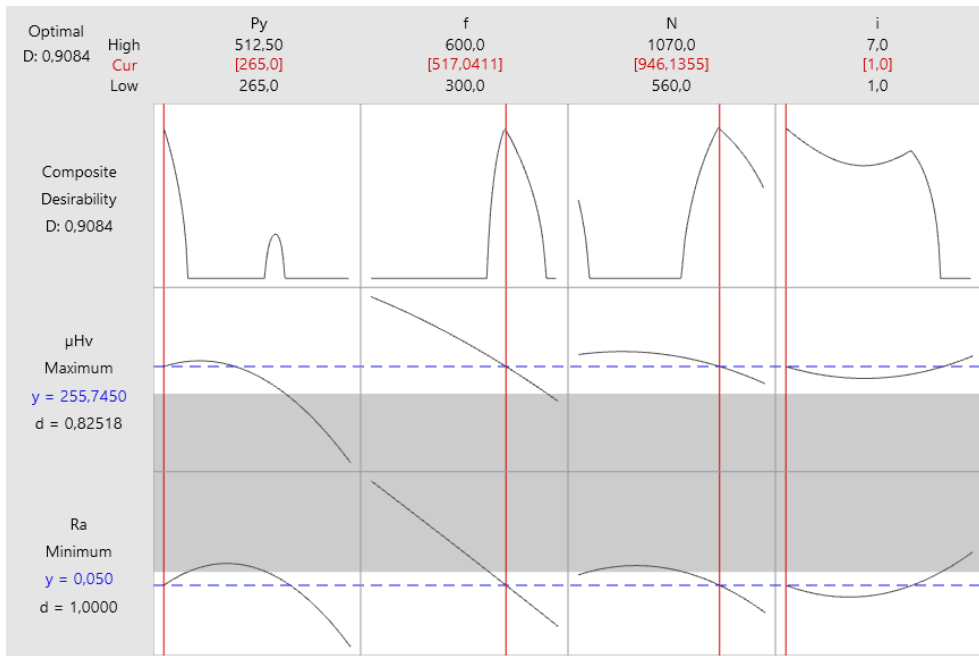


Fig. 8. Optimization graph of  $\mu H_v$  and  $R_a$

The results were collected and analyzed using the statistical software Minitab 19. By assigning equal weight and importance to both output responses, the burnishing regime that is expected to achieve a roughness ranging from 0.050 to 0.26  $\mu m$  and a micro hardness ranging from 204.67 to 266.57  $\mu H_v$  is characterized by level 1 of (Py) and (i), level 2 of (f), and level 3 of (N). Validating the adjustment of this regime yields a composite desirability value of  $D = 0.9084$ . Figure 8 graphically illustrates the optimal individual adjustments of the burnishing parameters to achieve the predetermined objective. Finally, the burnishing regime derived from the DFA was experimentally evaluated for confirmation. The results are satisfactory, considering the achieved surface roughness ( $R_a = 0.07 \mu m$ ) and microhardness ( $\mu H_v = 265$ ). These values are awfully close to those predicted by the regression models, demonstrating an improvement of 97.51% in surface roughness and a 40% increase in microhardness.

### 3.5. Effect of Burnishing on Corrosion Resistance

The experiments were performed on specimens in both their original machined condition and their burnished condition, utilizing various magnitudes of the burnishing force (Py) and feed rate (f) in accordance with a comprehensive, all-encompassing experimental design known as a full-factorial multifactorial design (Type 2<sup>2</sup>) [29]. The corrosion resistance was characterized by the polarization curve of API 5L X52 steel: Polarization curve of API 5L X52 steel- Tafel analysis and Open Circuit Potential (OCP) (Figure 9 and 10). Additionally, the Polarization Resistance ( $R_p$ ) can be related to the corrosion current through the Stern and Geary relationship. (Eq. 7)[39]:

$$I_{corr} = \frac{1}{R_p} \times \frac{\beta_a \times \beta_c}{2.303(\beta_a + \beta_c)} \quad (7)$$

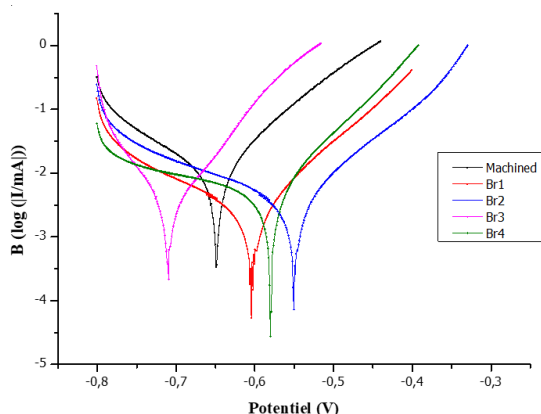


Fig. 9. Polarization curve of API 5L X52 steel– Tafel analysis [29]

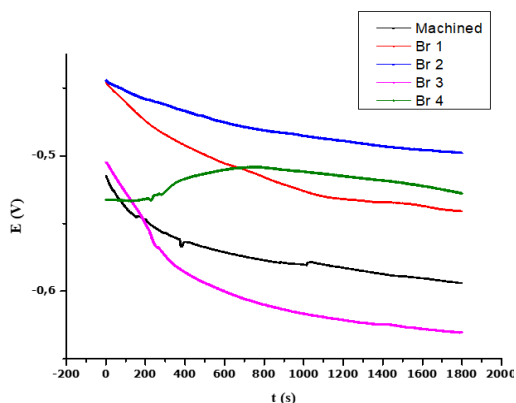


Fig. 10. Open Circuit Potential (OCP) Curve[29]

Polarization curve of API 5L X52 steel– Tafel analysis figure 9 show a rightward deviation for the burnished curves compared to the curve of the machined sample. This deviation is more pronounced for the parameters  $P_y = 430 \text{ N}$  and  $f = 500 \text{ mm/min}$  (Br2). Table 8 presents the results of the corrosion tests conducted on samples in the machined and burnished states. Figure 10 shows the evolution of the corrosion potential for samples immersed in a saline solution with NaCl. Over time, the corrosion potential decreases regardless of the treatment. The burnished curves are located above the curve of the machined sample, with a rapid drop in the corrosion potential within the first 200 seconds. Beyond this period, the curves continue to decrease with a less steep slope, while maintaining the same trend. Except for the sample treated with a burnishing force ( $P_y$ ) of 430 N and feed rate ( $f$ ) of 400 mm/min, the other combinations of burnishing parameters have a higher potential ( $E$ ). The optimal combination to achieve the highest corrosion potential is  $P_y = 430 \text{ N}$  and  $f = 500 \text{ mm/min}$ .

The reduction of  $R_p$  gain on X52 steel from 318 to 109% for both low and high levels of  $P_y$  can be achieved by increasing the value of  $f$ . To obtain the best possible corrosion resistance, it is essential to apply burnishing on low  $P_y$  and  $f$  values, which results in  $R_p = 14.17 \Omega$ . The use of RSM has enabled the identification of a linear prediction model of corrosion resistance, given by equation 6, which indicates that the burnishing force has a preponderant influence compared to the feed (fig 11 and 12). Additionally, an interaction between these two parameters has been observed, emphasizing the importance of

considering both factors in the burnishing process to achieve optimal corrosion resistance. Consequently, it is recommended that further research be done to determine the optimal values of  $P_y$  and  $f$ , which will lead to better corrosion resistance and overall durability of X52 steel [29].

Table 8. Electrochemical parameters of API 5L X52 steel

N°	Treatment	$E_{COR}$ (mv)	$I_{COR}$ ( $\mu A$ )	$\beta_c$ (mv)	$\beta_a$ (mv)	$R_p$ ( $\Omega$ )	(%)
M	Machined	-606.379	7.278	200	82.9		Ref
Br1	Br (265-400)	-603.725	1.538	132.7	84.9	14.617	318
Br2	Br (430-500)	-546.650	2.892	210.9	94.8	6.048	73
Br3	Br (430-400)	-710.564	1.824	46.5	61.1	6.285	80
Br4	Br (265- 500)	-577.445	3.644	300.6	77.0	7.304	109

$$R_p = 8.564 - 2.397X_1 - 1.88X_2 + 1.769X_1X_2 \quad [29] \quad (5)$$

It can be observed that the burnishing process has a positive effect on the corrosion resistance of API 5L X52 steel, as evidenced by the decrease in  $I_{CORR}$  and the consequent increase in  $R_p$  compared to the machined state (Table 8). The burnishing condition, characterized by  $P_y=265$  N and  $f=400$  mm/min, offers the highest  $R_p$  value of 14.617 A with a gain of 318% in  $R_p$ . However, increasing the  $P_y$  value from 265 N to 430 N reduces the  $R_p$  values, regardless of the  $f$  value. Similarly, increasing the  $f$  value also reduces the  $R_p$  gain from 318% to 109% (fig 13)[29].

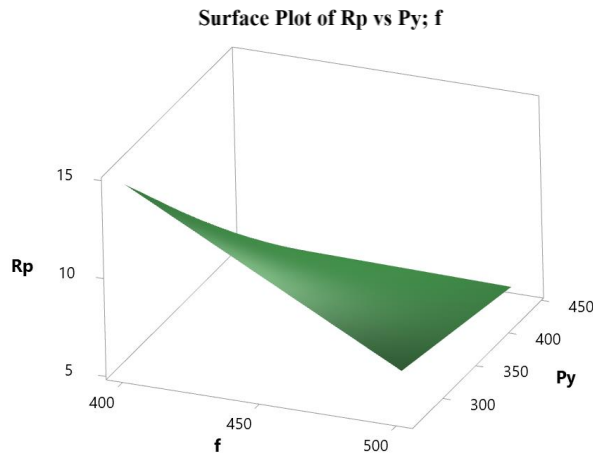


Fig. 11. Surface plot of  $R_p$  [29]

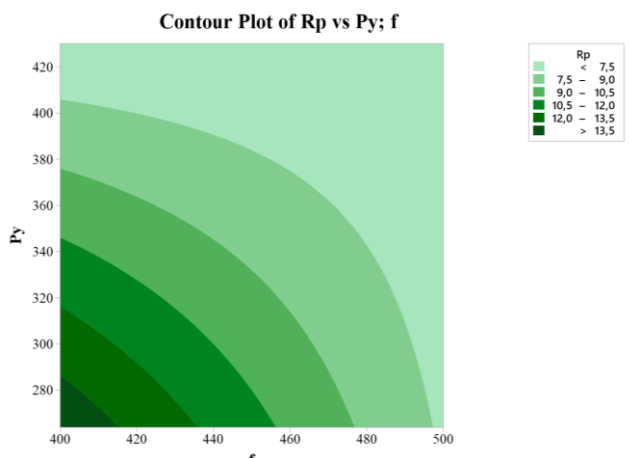


Fig. 12. Contour plot of Rp [29]

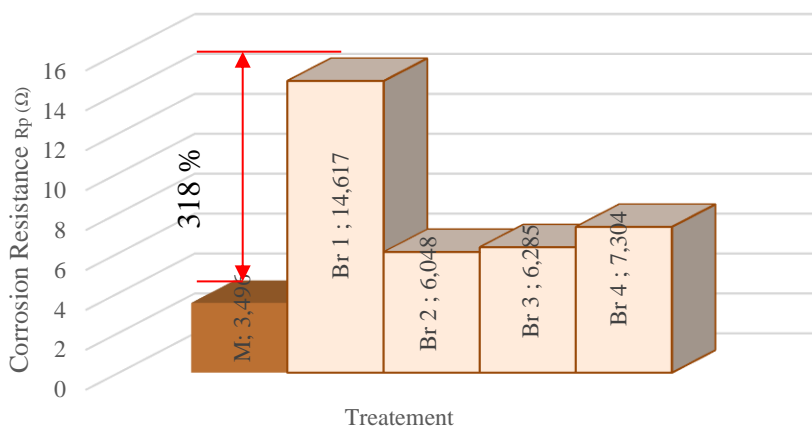


Fig. 13. Effect of burnishing parameters on corrosion resistance (Rp)

### 3.6. Microscopic Observations

Figure 14 and 15 present images acquired through scanning electron microscopy, offering insights into the corroded surfaces under examination. These visual representations distinctly depict variations in corrosion patterns, primarily emphasizing the contrasting effects of machining and burnishing processes on the material's surface. Specifically, these images underscore that corrosion tends to be more prominent on the machined surface, manifesting within the recesses of the machining asperities. In contrast, when the burnishing process is applied, it leads to a significant smoothing of these asperities, thereby reducing surface roughness [29]. This reduction in surface roughness, in turn, contributes to a noteworthy decrease in corrosion susceptibility. When burnishing is conducted with a force of 265 N and a feed rate of 500 mm/min, the resulting surface is the cleanest in terms of corrosion attack.



Fig. 14. Evolution of corrosion resistance ( $R_p$ ) before and after corrosion tests for unburnished samples[29].

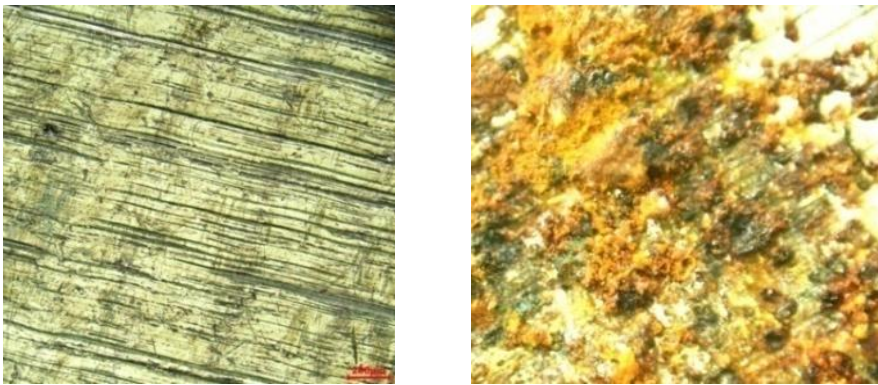


Fig. 15. Evolution of corrosion resistance ( $R_p$ ) before and after corrosion tests for burnished samples[29]

## 5. Conclusions

After subjecting the API 5L X52 steel to ball burnishing under various conditions, the following conclusions can be drawn:

- This study focused on the mechanical surface treatment of API 5L X52 steel, emphasizing the outer surface of the pipeline. It also presented a bespoke static device capable of treating both cylindrical and prismatic surfaces, highlighting its versatility and potential impact.
- The optimal burnishing parameters for plane surface burnishing were determined by conducting the process using the Taguchi L16 experimental design, S/N analysis. The surface roughness ( $R_a$ ) of the sample can be improved from approximately 0.26 to 0.05  $\mu\text{m}$  using the optimal ball burnishing parameters. The Vickers microhardness of the tested sample was improved from 204.67 to 266.57 after the burnishing process.
- The use of the Taguchi experimental design allowed for accurate modelling and prediction of the roughness and microhardness responses. The obtained models showed excellent correlation with the experimental results, with appreciable determination coefficients. The utilization of Analysis of Variance (ANOVA) based

on Signal-to-Noise (S/N) ratio has provided a quantitative insight into the influence of burnishing process parameters on both surface roughness and microhardness.

- Regarding surface roughness, the ANOVA reveals that the force applied ( $P_y$ ) and the feed rate ( $f$ ) play pivotal roles, contributing 37% and 32% to the observed variance, respectively. In contrast, spindle speed ( $N$ ) and the number of passes ( $i$ ) have relatively minor effects, with contributions of 8% and 12%, respectively. A portion of the remaining variance is attributed to error, comprising 11% of the total variance.
- Similarly, the ANOVA analysis for microhardness results underscore the dominant role of burnishing force ( $P_y$ ) and feed rate ( $f$ ) in minimizing surface roughness, contributing a significant combined effect of 81%. In contrast, spindle speed ( $N$ ) and the number of passes ( $i$ ) exhibit limited impact, accounting for only 8% of the variance collectively. These findings emphasize the critical importance of optimizing burnishing force and feed rate to achieve desired surface roughness improvements.
- Multi-objective optimization inspired by DFA revealed the following regime:  $P_y = 265$  N;  $f = 500$  mm/min;  $N = 900$  rpm; and  $i = 1$ . This burnishing regime yielded a surface roughness of  $R_a = 0.07$   $\mu\text{m}$  and a microhardness of  $\mu\text{Hv} = 265$ . These values are awfully close to those predicted by the regression models, demonstrating an improvement of 97.51% in surface roughness and a 40% increase in microhardness.
- The findings of the study indicate that ball burnishing can be deemed as a significant technique to enhance the corrosion resistance of API 5L X52 steel. Based on the outcome of the experiment, it is evident that the impact of burnishing results in a noteworthy surge of up to 318% in the corrosion resistance. Thus, it can be inferred that the implementation of ball burnishing can be an effective strategy to protect steel against corrosion.

## Acknowledgement

The authors would like to express their sincere appreciation to the Research Laboratory of Advanced Technology in Mechanical Production (LRATPM), Mechanical Engineering Department, at Badji Mokhtar-Annaba University. Their constant motivation and support throughout the investigations were invaluable. Additionally, the authors extend their heartfelt gratitude to SARL AVA CRISTAL for their assistance with specimen preparation. Special thanks are also due to the staff of the mechanical laboratory of TSS at the Algerian steel company in El-Hadjar, Annaba, for their collaboration in furnishing the materials and preparing the specimens.

## Nomenclature

- Symbols:
- $A$  Elongation (%)
- $E_{\text{corr}}$  Corrosion potential (mV)
- $f$  Burnishing (mm/min)
- $I_{\text{corr}}$  Corrosion current ( $\mu\text{A}$ )
- $i$  Number of passes
- $N$  Spindle speed (rpm)
- $P_y$  Burnishing force (kgf)
- $R_e$  Average yield strength (MPa)
- $UTS$  Ultimate tensile strength (MPa)
- $R_a$  Surface roughness ( $\mu\text{m}$ )
- $\mu\text{Hv}200$  Surface Vickers Microhardness

- $R_p$  Polarization resistance to corrosion (ohms)
- $\beta$  Potential difference between cathode and anode
- $\beta_a$  Sample polarization (mV)
- $\beta_c$  Reference measurement cell polarization (mV)
- $\eta_{Ra}$  Signal to noise Ratio for roughness
- $\eta_{\mu Hv}$  Signal to noise Ratio for microhardness

### Abbreviations:

- DFA Desirability function approach
- OCP Open circuit potential
- MABB Magnetic Assisted Ball Burnishing
- MST Mechanical surface treatment
- RSM Response surface methodology
- SEM Scanning electron microscopy
- SPD Superficial plastic deformation
- 

### References

- [1] Shao X. Research on the Steel for Oil and Gas Pipelines in Sour Environment. MATEC Web of Conferences, vol. 238, EDP Sciences; 2018. <https://doi.org/10.1051/mateconf/201823804010>
- [2] Al-Janabi YT. An Overview of Corrosion in Oil and Gas Industry: Upstream, Midstream, and Downstream Sectors. 2020.
- [3] Ma Q, Tian G, Zeng Y, Li R, Song H, Wang Z, et al. Pipeline in-line inspection method, instrumentation and data management. Sensors 2021;21. <https://doi.org/10.3390/s21113862>
- [4] Shehata MF, El-Shamy AM. Hydrogen-based failure in oil and gas pipelines a review. Gas Science and Engineering 2023;115:204994. <https://doi.org/10.1016/j.IGSCE.2023.204994>
- [5] Mahmoodian M, Li CQ. Stochastic failure analysis of defected oil and gas pipelines. Handbook of Materials Failure Analysis with Case Studies from the Oil and Gas Industry 2016:235–55. <https://doi.org/10.1016/B978-0-08-100117-2.00014-5>
- [6] Song CL, Liu XB, Pan X, Chen QG, Wang P, Fang Y. Failure Analysis of the Leakage and Ignition of an Oil–Gas Mixture Transportation Pipeline. Journal of Failure Analysis and Prevention 2022;22. <https://doi.org/10.1007/s11668-021-01279-4>
- [7] Ranjbar K, Alavi Zaree SR. Longitudinal fracture and water accumulation at 6 o'clock position of an API 5L X52 oil pipeline. Eng Fail Anal 2021;129. <https://doi.org/10.1016/j.engfailanal.2021.105691>
- [8] Dao U, Sajid Z, Zhang Y. Risk Assessment of Oil and Gas Pipelines Failure in Vietnam. International Journal of Engineering and Technology 2023;15. <https://doi.org/10.7763/ijet.2023.v15.1215>
- [9] Gharbi F, Sghaier S, Hamdi H, Benameur T. Ductility improvement of aluminum 1050A rolled sheet by a newly designed ball burnishing tool device. International Journal of Advanced Manufacturing Technology 2012;60:87–99. <https://doi.org/10.1007/s00170-011-3598-6>
- [10] López De Lacalle LN, Lamikiz A, Muñoz J, Sánchez JA. Quality improvement of ball-end milled sculptured surfaces by ball burnishing. Int J Mach Tools Manuf 2005;45:1659–68. <https://doi.org/10.1016/j.ijmactools.2005.03.007>
- [11] Tadic B, Todorovic PM, Luzanin O, Miljanic D, Jeremic BM, Bogdanovic B, et al. Using specially designed high-stiffness burnishing tool to achieve high-quality surface finish.

- International Journal of Advanced Manufacturing Technology 2013;67:601-11. <https://doi.org/10.1007/s00170-012-4508-2>
- [12] Jerez-Mesa R, Travieso-Rodríguez JA, Landon Y, Dessein G, Lluma-Fuentes J, Wagner V. Comprehensive analysis of surface integrity modification of ball-end milled Ti-6Al-4V surfaces through vibration-assisted ball burnishing. J Mater Process Technol 2019;267:230-40. <https://doi.org/10.1016/j.jmatprotec.2018.12.022>
- [13] Maximov JT, Duncheva G V., Anchev AP, Ichkova MD. Slide burnishing—review and prospects. International Journal of Advanced Manufacturing Technology 2019;104:785-801. <https://doi.org/10.1007/s00170-019-03881-1>
- [14] Jerez-Mesa R, Travieso-Rodríguez JA, Gomez-Gras G, Lluma-Fuentes J. Development, characterization and test of an ultrasonic vibration-assisted ball burnishing tool. J Mater Process Technol 2018; 257:203-12. <https://doi.org/10.1016/j.jmatprotec.2018.02.036>
- [15] Zhou Z yu, Yu G lei, Zheng Q yang, Ma G zheng, Ye S bin, Ding C, et al. Wear behavior of 7075-aluminum after ultrasonic-assisted surface burnishing. J Manuf Process 2020;51:1-9. <https://doi.org/10.1016/j.jmapro.2020.01.026>
- [16] Saldaña-Robles A, De La Peña JÁD, De Jesús Balvantín-García A, Aguilera-Gómez E, Plascencia-Mora H, Saldaña-Robles N. Ball burnishing process: State of the art of a technology in development. Dyna (Spain) 2017;92:28-33. <https://doi.org/10.6036/7916>
- [17] Tugay IO, Hosseinzadeh A, Yapici GG. Hardness and wear resistance of roller burnished 316L stainless steel. Mater Today Proc, vol. 47, Elsevier Ltd; 2021, p. 2405-9. <https://doi.org/10.1016/j.matpr.2021.04.363>
- [18] Jayaraman N, Prevéy PS, Ravindranath R. Low Plasticity Burnishing (LPB) Treatment to Mitigate FOD and Corrosion Fatigue Damage in 17-4 PH Stainless Steel. n.d.
- [19] Al-Qawabeha UF, Al-Qawabah SM. Effect of roller burnishing on pure aluminum alloyed by copper. Industrial Lubrication and Tribology 2013;65:71-7. <https://doi.org/10.1108/00368791311303438>
- [20] Thorat SR, Thakur AG. Analysis of surface roughness and wear resistance in low plasticity burnishing process using multi-objective optimization technique. Mater Today Proc, vol. 41, Elsevier Ltd; 2019, p. 1082-8. <https://doi.org/10.1016/j.matpr.2020.07.543>
- [21] Kovács Z. The investigation of tribological characteristics of surface improved by magnetic polishing and roller burnishing. Procedia Eng, vol. 149, 2016. <https://doi.org/10.1016/j.proeng.2016.06.654>
- [22] Al-Qawabeha U, Al-Rawajfeh AE, Al-Shamaileh E. Influence of roller burnishing on surface properties and corrosion resistance in steel. Anti-Corrosion Methods and Materials 2009;56:261-5. <https://doi.org/10.1108/00035590910989552>
- [23] Jawahar M, Suresh kumar J, Srikanth M, Ismail S. Experimental Investigation of Ball Burnishing Process Parameters Optimization for Al 5083 Using Taguchi Method. Lecture Notes in Mechanical Engineering, 2020. [https://doi.org/10.1007/978-981-15-1124-0\\_17](https://doi.org/10.1007/978-981-15-1124-0_17)
- [24] Vaishya RO, Sharma V, Mishra V, Gupta A, Dhanda M, Walia RS, et al. Mathematical Modeling and Experimental Validation of Surface Roughness in Ball Burnishing Process. Coatings 2022;12. <https://doi.org/10.3390/coatings12101506>
- [25] Pathade HP, Gupta DrMK, Kumar DrN, Pathade MP, Wakchaure PB, Gadhave SN, et al. A Review on Surface Integrity of Ball Burnishing Process. International Journal of Research Publication and Reviews 2022. <https://doi.org/10.55248/gengpi.2022.3.10.3>
- [26] Yadav PS, Ghatge DA. Performance Improvement of Roller Burnishing Process- A Review. IARJSET 2017;4. <https://doi.org/10.17148/iarjset/ncdmete.2017.34>
- [27] Raza A, Kumar S. A critical review of tool design in burnishing process. Tribol Int 2022;174. <https://doi.org/10.1016/j.triboint.2022.107717>

- [28] ASTM Standards. ASTM: A370 /ASME SA-370 Standard Test Methods and Definitions for Mechanical Testing of Steel Products<sup>1</sup>. American Society for Testing and Materials 2016.
- [29] Hamadache Hamid, Belabend Selma, Phamdonhat Quang. Improved Corrosion Resistance Of Ball Burnished Api X52 Steel. The 2nd World Energy Storage Conference (WESC-2022), December 18-21, 2022, Istanbul, Turkiye, Istanbul, Turkiye: 2022.
- [30] Bounouara A, Hamadache H, Amirat A. Investigation on the effect of ball burnishing on fracture toughness in spiral API X70 pipeline steel. International Journal of Advanced Manufacturing Technology 2018;94. <https://doi.org/10.1007/s00170-017-1181-5>.
- [31] Lieth HM, Al-Sabur R, Jassim RJ, Alsahlani A. Enhancement of corrosion resistance and mechanical properties of API 5L X60 steel by heat treatments in different environments. Journal of Engineering Research (Kuwait) 2021;9:428–40. <https://doi.org/10.36909/jer.14591>
- [32] Garcia MP, de Souza JS, Glover C, Ansell P, Williams G, Mantovani GL, et al. Global and Local Corrosion of Welded Joints of High-Strength Low-Alloy Automotive Steel. Corrosion 2021;77:562–74. <https://doi.org/10.5006/3718>
- [33] Alraeeini AS, Nikbakht E, Ismail MC. Square Steel Tube Impressed Current Corrosion Rate in Term of Linear Polarization Resistance (LPR) Method. Lecture Notes in Civil Engineering, vol. 139 LNCE, 2021. [https://doi.org/10.1007/978-981-33-6560-5\\_14](https://doi.org/10.1007/978-981-33-6560-5_14)
- [34] Díaz-Jiménez V, Arellanes-Lozada P, Likhanova N V., Olivares-Xometl O, Chigo-Anota E, Lijanova I V., et al. Investigation of Sulfonium-Iodide-Based Ionic Liquids to Inhibit Corrosion of API 5L X52 Steel in Different Flow Regimes in Acid Medium. ACS Omega 2022;7:42975–93. <https://doi.org/10.1021/acsomega.2c05192>
- [35] Nikitasari A, Astuti IM, Musabikha S, Kusumastuti R, Prifiharni S, Priyotomo G. Chasew (Anacardium Occidentale) Leaves Extract as Green Corrosion Inhibitor of API 5L X52 in Acidic Media. Trends in Sciences 2023;20. <https://doi.org/10.48048/tis.2023.4733>
- [36] Asmare A, Al-Sabur R, Messele E. Experimental investigation of friction stir welding on 6061-t6 aluminum alloy using taguchi-based gra. Metals (Basel) 2020;10:1–21. <https://doi.org/10.3390/met10111480>
- [37] Trembach B, Grin A, Turchanin M, Makarenko N, Markov O, Trembach I. Application of Taguchi method and ANOVA analysis for optimization of process parameters and exothermic addition (CuO-Al) introduction in the core filler during self-shielded flux-cored arc welding n.d. <https://doi.org/10.1007/s00170-021-06869-y>
- [38] Fajdek-Bieda A. The use of the desire function analysis (DFA) of selected unit processes in chemical technology. Procedia Comput Sci, vol. 207, Elsevier B.V.; 2022, p. 810–8. <https://doi.org/10.1016/j.procs.2022.09.136>
- [39] Han ZY, Huang XG. Stress corrosion behavior of X80 pipeline steel in the natural seawater with different dissolved oxygen contents. Frattura Ed Integrita Strutturale 2019;13:21–8. <https://doi.org/10.3221/IGF-ESIS.50.03>